Insights into the Structural and Chemical Modifications of Nb Additive on TiO_2 Nanoparticles

Ana M. Ruiz,* G. Dezanneau, J. Arbiol, A. Cornet, and Joan R. Morante

EME, Departament d'Electronica, Universitat de Barcelona, C/ Marti i Franquès, 1, E-08028 Barcelona, Spain

Received November 5, 2003. Revised Manuscript Received December 22, 2003

The solid solution $Nb_xTi_{1-x}O_{2+\delta}$ has been synthesized by a sol−gel method with $0.0 \leq x \leq 0.1$. Structural and microstructural properties have been studied by XPS, XRD, Raman spectroscopy, and TEM as a function of the Nb/Ti atomic ratio and thermal treatment temperature (600−900 °C). XRD analyses showed that a percentage of the nominal added Nb was assimilated in substitutional Ti sites in the bulk of TiO_2 adopting a pentavalent state. On the other hand, XPS detected a high concentration of Nb at the surface. On the basis of the careful analysis of the XRD and XPS spectra it is reasonable to assume that the concentration of Nb at the surface of the nanoparticles is higher than that in the bulk, especially for rutile, giving a U-shaped Nb concentration profile. The niobium incorporation stabilizes the titania obstructing the diffusion of anatase-type surface atoms, which prevents grain coarsening and phase transformation. The solubility limit of niobium into titania is greater for the anatase phase ($x > 0.1$) than for the rutile phase ($x = 0.06$). Once the solubility limit of Nb atoms is surpassed, a ternary phase ascribed to $TiNb_2O_7$ has been detected. In addition, the crystallite sizes and the percentage of rutile phase were quite similar for Nb contents above the solubility limit. XRD and XPS measurements suggest that niobium mainly enters into titania phase with valence +5, while Ti maintains its higher oxidation state (4+), the extra charge being thus partially compensated by titanium vacancies. As derived from XPS analyses in the core levels and the valence band regions, the addition of Nb resulted in a displacement of the Fermi level toward the conduction band. In consequence, the Nb-altered samples presented a more marked n-type feature, as compared with that of the bare TiO_2.

Introduction

Nanosized ceramics with average grain sizes lower than 100 nm have generated considerable interest due to the improvements in a variety of properties (strength, toughness, catalytic reactivity, gas detection capability, etc.) that are expected to result from grain size adjustment.[1−4] In gas sensors, special attention has been focused on metal−oxide semiconductors, which change their conductivity depending on the gas in contact with their surface.[5] TiO_2 is one of the ceramics with a wide range of applications in solid-state chemistry, surface science, photocatalysis, pigments, or gas sensors.[6−9] The ionic conductivity of TiO_2 has been used to develop commercial oxygen sensors in lambda devices,[10] and its electronic conductivity offers promising features for pollutant gas detection.[11]

Usually, for better sensing performances, titania has been modified with a variety of additives, such as Cr, La, W, Mo, Fe, Pt, or Nb.[12−16] It has been shown that, among them, Nb is effective for enhancing the sensitivity and shortening the response time in TiO_2 oxygen gas sensors,[17] giving a satisfactory response to NO_2 in environmental monitoring sensors,[18] or improving the photosensitivity of TiO_2 to NO.[19]

* To whom correspondence should be addressed. E-mail: aruiz@el.ub.es. Phone/fax: +34 93 402 11 48.

(1) Bonini, N.; Carotta, M. C.; Chiorino, A.; Guidi, V.; Malagu, C.; Martinelli, G.; Paglialonga, L.; Sacerdoti, M. *Sens. Actuators B* **2000**, *68*, 274.
(2) Kaya, C.; He, J. Y.; Gu, X.; Butler, E. G. *Microporous Mesoporous Mater.* **2002**, *54*, 37.
(3) Baik, N. S.; Sakai, G.; Shimanoe, K.; Miura, N.; Yamazoe, N. *Sens. Actuators B* **2000**, *65*, 97.
(4) Dabhade, V. V.; Rama Mohan, T. R.; Ramakrishnan, P. *Appl. Surf. Sci.* **2001**, *182*, 390.
(5) Williams, D. E. *Sens. Actuators B* **1999**, *57*, 1.
(6) Wang, C. C.; Zhang, Z.; Ying, J. Y. *Nanostruct. Mater.* **1997**, *9*, 583.
(7) Croll, S. *Prog. Org. Coat.* **2002**, *44*, 131.
(8) Kavan, L.; Grätzel, M.; Gilbert, S. E.; Klemenz, C.; Scheel, H. J. *J. Am. Chem. Soc.* **1996**, *118*, 6716.
(9) Akbar, S. A.; Younkman, L. B. *J. Electrochem. Soc.* **1997**, *149* (5), 1750.
(10) Just Lambda. http://www.lambdasensor.com/.
(11) Carotta, M. C.; Martinelli, G.; Crema, L.; Malagu, C.; Merli, M.; Ghiotti, G.; Traversa, E. *Sens. Actuators B* **2001**, *76*, 336.
(12) Ruiz, A.; Sakai, G.; Cornet, A.; Shimanoe, K.; Morante, J. R.; Yamazoe, N. *Sens. Actuators B* **2003**, *93*, 509.
(13) Dutta, P. K.; Ginwalla, A.; Hogg, B.; Patton, B. R.; Chwieroth, B.; Liang, Z.; Gouma, P.; Mills, M.; Akbar, S. *J. Phys. Chem. B* **1999**, *103*, 4412.
(14) Bregani, F.; Casale, C.; Depero, L. E.; Natali-Sora, I.; Roba, D.; Sangaletti, L.; Toledo, G. P. *Sens. Actuators B* **1996**, *31*, 25.
(15) Comini, E.; Guidi, V.; Frigeri, C.; Ricco, I.; Sberveglieri, G. *Sens. Actuators B* **2001**, *77*, 16.
(16) Ruiz, A.; Arbiol, J.; Cirera, A.; Cornet, A.; Morante, J. R. *Mater. Sci. Eng. C* **2002**, *19*, 105.
(17) Sharma, R. K.; Bhatnagar, M. C.; Sharma, G. L. *Sens. Actuators B* **1998**, *46*, 194.
(18) Carotta, M. C.; Ferroni, M.; Gnani, D.; Guidi, V.; Merli, M.; Martinelli, G.; Casale, M. C.; Notaro, M. *Sens. Actuators B* **1999**, *58*, 310.

10.1021/cm0351238 CCC: $27.50
Published on Web 02/06/2004

Up to now, many efforts have been devoted to describe the TiO_2/Nb system in terms of structural and electronic properties. Gao and co-workers grew epitaxial films of Nb-modified TiO_2 by molecular beam epitaxy (MBE)[20,21] and metal−organic chemical vapor deposition.[22,23] Up to 40 at. % of Nb, a homogeneous solid solution with the rutile structure and free of any secondary phases was formed, in which Nb incorporated substitutionally at Ti sites and assumed a 4+ oxidation state in the lattice. Substitutional Nb in TiO_2 introduces an additional valence electron per Nb cation. In the MBE-grown films, they found that the additional Nb 4d valence electron created a new density of occupied states that fell in the valence band region. The extra valence electrons were expected to form a Nb-derived nonbonding band in the bulk, whereas in the surface they were expected to remain localized in Nb dangling bond states. These electrons could be excited to form electron−hole pairs, which could be responsible for the enhanced surface photochemical activity. In contrast, Morris et al.,[24] working in the case of low Nb concentrations, found a new state in the band gap of rutile, and these extra Nb valence electrons were mainly localized on Ti rather than Nb. They suggested that in the MBE-grown films the Nb^{4+} is inevitably oxidized to Nb^{5+} and the charge is compensated by cation vacancies or oxygen interstitials.

Valigi et al.[25] studied the system in the composition range $0.0 < x < 0.1$ for different heat treatment conditions. When the samples were heated under vacuum, niobium entered in solid solution in the valence 5+ and the extra positive charge was compensated by the creation of an equivalent amount of Ti^{3+}. If the treatment was done in an oxidizing atmosphere, the maximum solubility of Nb^{5+} into rutile form was 6.6 cation atomic percent, above which Nb excess was segregated as $TiNb_2O_7$ and Ti^{3+} was oxidized to Ti^{4+} yielding a compensation of Nb^{5+} by cation vacancies. The secondary phase of $TiNb_2O_7$ has been also observed by Zakrzewska et al.[26] when Nb content exceeded 6 at. %.

Antonio et al.[27] used synchrotron radiation for X-ray absorption spectroscopy. In particular, they performed X-ray absorption near edge structure (XANES) experiments, which can provide information about vacant orbitals, electronic configuration, oxidation state, and site symmetry of the absorbing atom. They studied the coordination and valence of niobium in $Nb_xTi_{1-x}O_2$ solid solutions for $0.1 < x < 1.0$ prepared under reducing atmosphere and found that the Nb cation valence increases from 4+ to 5+ with decreasing Nb concentration and suggested that the $4d^1$ electrons of Nb^{4+} are donated to or shared with Ti^{4+} ($3d^0$) at low Nb concentration, therefore increasing the valence of Nb from +4 to +5 due to this loss of electrons. As the Nb content increases, Nb ions interact with themselves and the $4d^1$ electrons are localized as Nb^{4+}.

In short, the introduction of Nb into titania can modify the microstructure of the base material, control crystallite growth mechanisms, and introduce electronic states at the surface or into the bulk of the grain giving rise to a modification of the material conductivity. Regarding the electronic states characterization, several perspectives and models can be found in the literature, mainly owing to the different procedures followed in the preparation of the samples, such as high or low concentration of additive, oxidizing or reducing treatment, synthesis based on wet chemical route or MBE, etc. Nevertheless, there are still few ideas about the way such effects contribute to the knowledge of the material prepared for gas sensing applications. In this regard, a detailed characterization of the morphological, structural, and electrical properties of a well-defined set of TiO_2/Nb nanoparticles (i.e., systematic studies of different niobium contents and synthesis temperatures) could contribute to a more accurate interpretation of the material characteristics and the gas sensing mechanisms.

In this scope, the present study aims to analyze the influence of niobium introduction, as well as of calcination treatment, on the TiO_2 properties from a material characteristics point of view, for TiO_2 nanoparticles obtained from a wet chemical route. It will provide us with the means toward a better understanding of the gas sensing behavior. For that purpose, nanopowders were prepared by sol−gel with various Nb/Ti ratios and synthesis temperatures, and analyzed by X-ray photoelectron spectroscopy (XPS), transmission electron microscopy (TEM), X-ray diffraction (XRD), and Raman spectroscopy. From these results, we tried to correlate the niobium content and synthesis temperature to the evolution of structural and electronic properties, for instance the crystallite size, the crystallographic phases, and the chemical states.

Experimental Section

The Nb-modified TiO_2 samples were synthesized through a sol−gel route starting from alkoxides precursors (titanium isopropoxide and niobium ethoxide). Because titanium isopropoxide easily precipitates with moisture, it was used as 0.5 M solution in 2-propanol. An appropriate volume of niobium ethoxide was added to this solution to get a concentration of 0, 2, 4, 6, 8, and 10% in Nb/Ti atomic ratio, i.e., to get $Nb_xTi_{1-x}O_{2+\delta}$ solid solutions with x equal to 0, 0.02, 0.04, 0.06, 0.08, and 0.1. The titanium−niobium alkoxide solution was then added dropwise under vigorous stirring to nitric acid aqueous solution. The stirring was maintained until a transparent solution was observed. Gellification of the sols was obtained by adding a weak alkaline aqueous solution (pH = 8). The white elastic gels were then dried at 80 °C and calcined under air. The thermal treatment was a heating ramp of 5 °C/min up to the holding temperature (600, 700, 800, and 900 °C) for 3 h, followed by a free cooling ramp.

X-ray diffraction measurements were performed on a Siemens D500 diffractometer, working with the Cu $K\alpha_{1,2}$ wavelength. Diffraction patterns were recorded at a lower scan rate from 20 to 30° in 2θ where main peaks of anatase and rutile phases are observed, to calculate crystallite size and percent-

(19) Kudo, M.; Kosaka, T.; Takahashi, Y.; Kokusen, H.; Sotani, N.; Hasegawa, S. *Sens. Actuators B* **2000**, *69*, 10.
(20) Gao, Y.; Liang, Y.; Chambers, S. A. *Surf. Sci.* **1996**, *348*, 17.
(21) Chambers, S. A.; Gao, Y.; Kim, Y. J.; Henderson, M. A.; Thevuthasan, S.; Wen, S.; Merkle, K. L. *Surf. Sci.* **1996**, *365*, 625.
(22) Gao, Y. *Thin Solid Films* **1999**, 346, 73.
(23) Gao, Y.; Thevuthasan, S.; McCready, D. E.; Engelhard, M. *J. Cryst. Growth* **2000**, *212*, 178.
(24) Morris, D.; Dou, Y.; Rebane, J.; Mitchell, C. E. J.; Egdell, R. G.; Law, D. S. L.; Vittadini, A.; Casarin, M. *Phys. Rev. B* **2000**, *61*, 13445.
(25) Valigi, M.; Cordischi, D.; Minelli, G.; Natale, P.; Porta, P.; Keijzers, C. P. *J. Solid State Chem.* **1988**, *77*, 255.
(26) Zakrzewska, K.; Radecka, M.; Rekas, M. *Thin Solid Films* **1997**, *310*, 161.
(27) Antonio, M. R.; Song, I.; Yamada, H. *J. Solid State Chem.* **1991**, *93*, 183.

age of phases. For the assessment of lattice effects on the normal vibration modes, Raman spectra were recorded on a Jobin-Yvon T6400 instrument with an Ar^+ laser source of 514 nm wavelength in a macroscopic configuration. The morphology of the powders was observed by transmission electron microscopy (TEM), which was carried out using a Phillips CM30 supertwin apparatus, operating at 300 kV with a 0.19-nm point resolution. X-ray photoelectron spectroscopy data were collected with a Physical Electronics 5500 spectrometer under a pressure of 10^{-9} Torr. XPS spectra were excited by monochromatized Al Kα X-ray source ($h\nu = 1486.6$ eV). Electron loss was compensated by a low-energy electron beam (20 mA current emission, 15 eV electron energy). Nevertheless, to avoid charge effects the spectra were fitted to get the right *C 1s* peak position (285.8 eV).

Results

To observe the morphology of the samples, some powders were suspended in an organic alcohol and deposited on a holey carbon membrane for TEM analyses. Figure 1 shows the TEM micrographs for the bare TiO_2 and the Nb-added TiO_2 with $x = 0.1$ heat-treated at 600 °C. In these pictures it is observed that the 600 °C calcined materials were formed of roughly spherical nanocrystalline particles, the size of which strongly depends on the niobium content. Bare TiO_2 calcined at 600 °C (Figure 1a) exhibited a poorer homogeneity in particles' size and shape than in the case of the Nb-modified powders (Figure 1b). In the case of the Nb-modified samples calcined at 600 °C we observed that the distribution of diameters is more uniform and the thermal-caused grain growth has been prevented. Similarly, we observed by TEM the samples calcined at 900 °C (not shown). At this high-temperature treatment, the Nb-modified samples also presented an average crystallite size smaller than that of the unmodified samples. However, the particle size distribution is more inhomogeneous than at lower temperatures. Moreover, as we will discuss later, the segregation of a ternary phase is produced from 800 °C on. This segregation reduces the amount of Nb effectively introduced in the titania lattice that could prevent the coalescence.

The average crystallite size for all the samples has been calculated from XRD diffractograms using the Debye−Scherrer equation. Figure 2 shows the evolution of sizes for the anatase phase at 600 and 700 °C, and for rutile at 600, 700, 800, and 900 °C. It is clearly shown how the Nb avoids crystallite coarsening. The growth inhibition is effective until $x = 0.06$ (6 at. % of Nb/Ti). Above this concentration, the crystallites have approximately the same size at a fixed calcination temperature. Anatase crystallites at 600 and 700 °C were smaller than 30 nm for all the Nb concentrations. These values are slightly lower than the results reported in ref 28 for the same conditions of Nb content and calcination temperature. Such discrepancies may be because of different sample processing performed.

In Figure 3, we present X-ray diffraction patterns for the series of samples synthesized at 600, 700, 800, and 900 °C. On these graphs, we identify the (101) diffraction peak of anatase (open circle in Figure 2a) at $2\theta = 25.30°$, and the (100) diffraction peak of rutile (cross

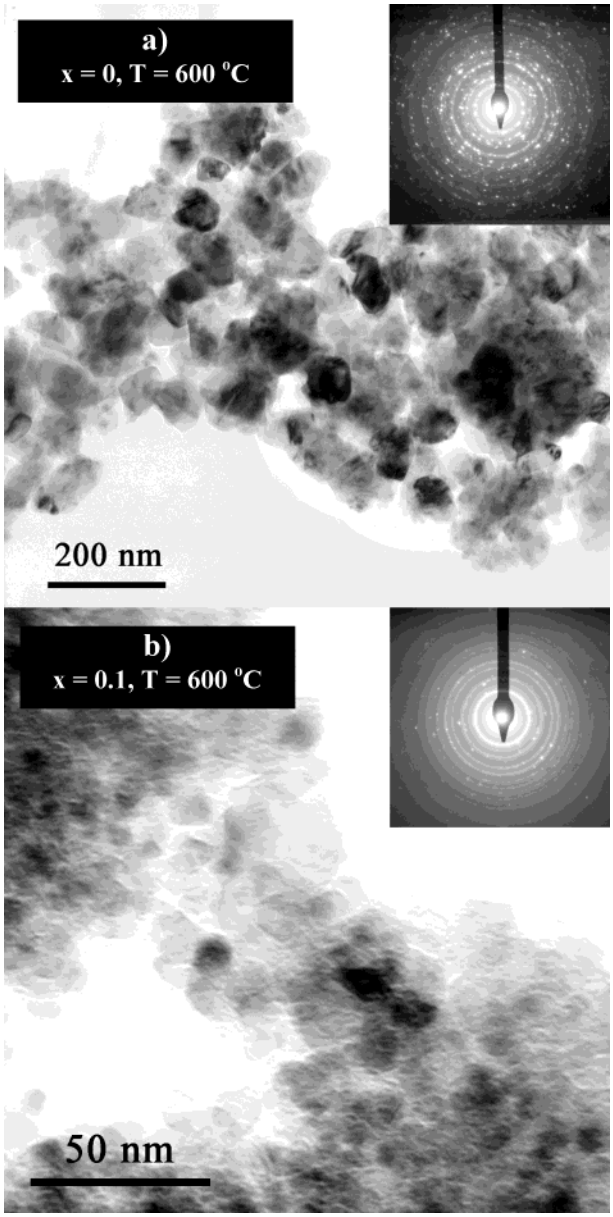

Figure 1. Transmission electron microscopy images and selected area diffraction patterns of nanopowder samples with Nb/Ti ratio (x) and synthesis temperature (T) of (a) $x = 0$, $T =$ 600 °C, and (b) $x = 0.1$, $T = 600$ °C.

symbol) at $2\theta = 27.4°$, which correspond to the most intense reflection of either phase. Samples synthesized at 600 °C present a mixture of anatase and rutile phases, with the rutile content diminishing with increasing niobium content. The bare TiO_2 has been totally converted to rutile at 700 °C, whereas the Nb-modified samples are still a mixture of phases, predominantly anatase, except for $x = 0.02$. At 800 and 900 °C the ternary phase $TiNb_2O_7$ has been observed for high Nb concentrations ($x \geq 0.08$). Samples synthesized at 900 °C present only the rutile form of TiO_2. The evolution of the titania crystallographic forms observed by XRD are in accordance with the Raman analyses. Figure 4 shows the Raman spectra of the samples synthesized at 600, 700, 800,and 900 °C. On these graphs, we identify the main Raman bands of anatase (full lines) at 138 cm^{-1} (E_g), 397 cm^{-1} (B_{1g}), 516 cm^{-1} (B_{1g}), and 639 cm^{-1} (E_g), and of rutile (dash lines) at 235 cm^{-1} (disorder or second-order scattering[29]),

(28) Ferroni, M.; Carotta, M. C.; Guidi, V.; Martinelli, G.; Ronconi, F.; Richard, O.; Van Dyck, D.; Van Landuyt, J. *Sens. Actuators B* **2000**, *68*, 140.

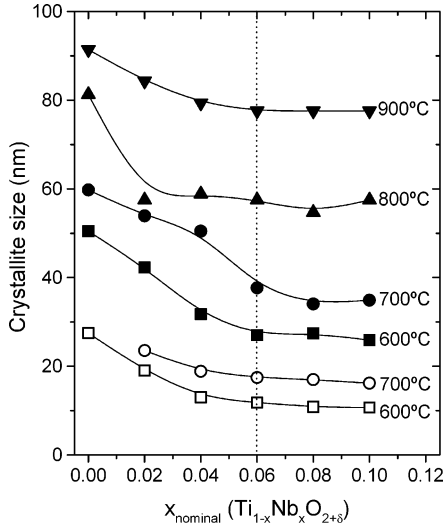

Figure 2. Evolution of crystallite size as a function of temperature and niobium content for both anatase (open symbols) and rutile (solid symbols).

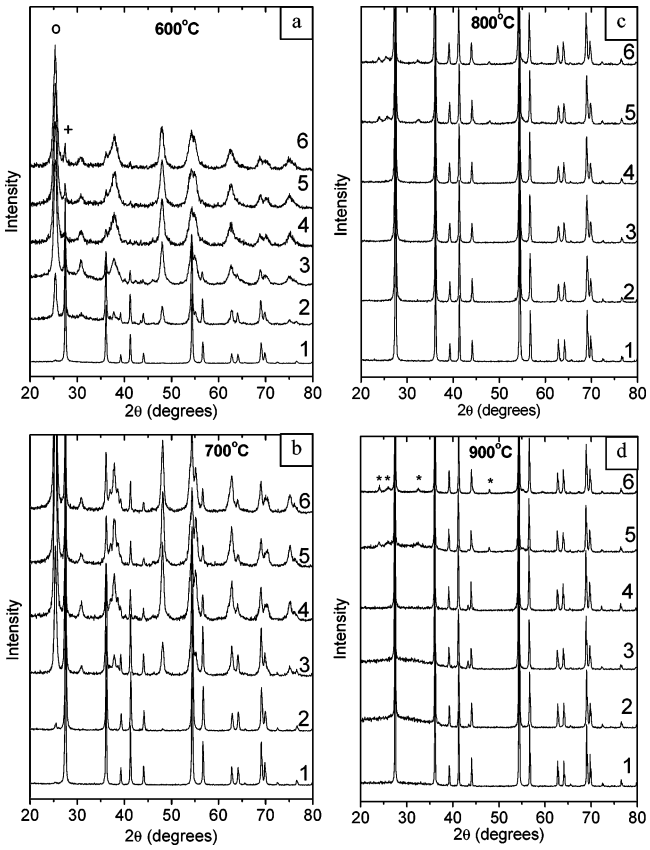

Figure 3. Evolution of X-ray diffraction patterns for Nb/Ti contents of $x = 0$ (1), $x = 0.02$ (2), $x = 0.04$ (3), $x = 0.06$ (4), $x = 0.08$ (5) and $x = 0.1$ (6), for samples synthesized at 600 (a), 700 (b), 800 (c), and 900 °C (d). Open circle in (a) corresponds to anatase, and cross corresponds to rutile; star symbols in (d) correspond to $TiNb_2O_7$.

449 cm^{-1} (E_g), and at 610 cm^{-1} (A_{1g}).[30] Both Raman and XRD data show that the increase of niobium content in TiO_2 hinders the anatase-to-rutile transformation.

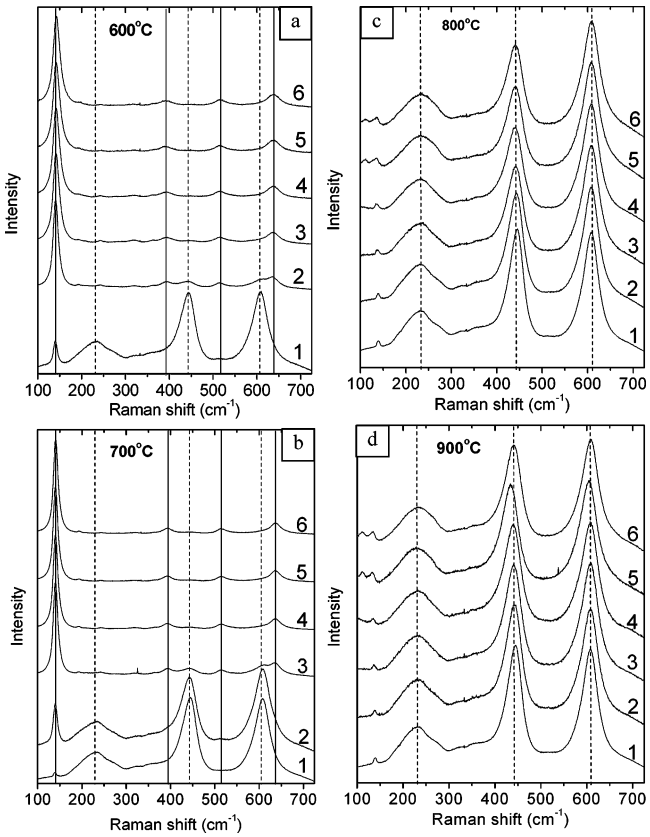

Figure 4. Evolution of Raman patterns for Nb/Ti contents of $x = 0$ (1), $x = 0.02$ (2), $x = 0.04$ (3), $x = 0.06$ (4), $x = 0.08$ (5), and $x = 0.1$ (6), for samples synthesized at 600 (a), 700 (b), 800 (c), and 900 °C (d). Solid lines correspond to anatase and dashed lines correspond to rutile.

To quantify the effect of Nb content on this structural transformation, we calculated from XRD and Raman spectra the relative amounts of anatase and rutile phases. First, we simulated the diffraction diagrams of a mixture of anatase and rutile phases using the program FULLPROF[31] for different anatase-to-rutile molar ratios. From these simulations, the rutile percentage versus the ratio of intensity of (110) rutile reflection I_R over the sum of I_R and the anatase (101) reflection I_A can be expressed as follows:

$$\left(\frac{\text{Rutile}}{TiO_2}\right)_{RX} = 1.369\frac{I_R}{I_A + I_R} - 0.369\left[\frac{I_R}{I_A + I_R}\right]^2 \quad (1)$$

It is necessary to state that this equation has been calculated for pure TiO_2 samples. Thus, to estimate the error in the case of niobium-added samples, simulations have also been performed assuming a 50:50 molar mixture of anatase and rutile with 10% (respectively 0%) of niobium in anatase and 0% (respectively 10%) in rutile. From these simulations, we evaluated the relative error on the calculated rutile percentage to be about 10%.

Similarly, the percentage of rutile can be determined from Raman spectra using the following equation:[32]

(29) Ocaña, M.; Fornés, V.; García-Ramos, J. V.; Serna, C. J. *J. Solid State Chem.* **1988**, *75*, 364.

(30) Tompsett, G. A.; Bowmaker, G. A.; Cooney, R. P.; Metson, J. B.; Rodgers, K. A.; Seakins, J. M. *J. Raman Spectrosc.* **1995**, *26*, 57.

(31) Rodriguez-Carvajal, J. *Powder Diffraction, Abstracts of the Satellite Meeting of the XV congress of the International Union of Crystallography, Toulouse 16−19 July*, 1990, 127.

(32) Gonzáles, R. J. *Raman, Infrared, X-ray and EELS studies of Nanophase Titania.* Ph.D. Thesis, Virginia Polytechnic Institute and State University, Blacksburg, Virginia, 1996.

$$\left(\frac{\text{Rutile}}{TiO_2}\right)_{\text{Raman}} = \frac{1}{1 + 0.038\frac{I_{140}}{I_{440}}} \quad (2)$$

where I_{140} refers to the more intense Raman band of anatase at roughly 140 cm^{-1}, and I_{440} refers to the more intense Raman band of rutile at 440 cm^{-1}. In this case also, the equation has been proposed for pure TiO_2.

These results are presented in Figure 5, where we show the evolution of rutile percentage as a function of synthesis temperature and niobium content, calculated from both XRD and Raman spectroscopy data. First of all, we can see that there is quite a good agreement between the two techniques, confirming the validity of the assumed approximations. We observe that the introduction of niobium into TiO_2 displaces the anatase to rutile transformation to higher temperature. For instance, after a thermal treatment of 3 h at 600 °C, the unmodified sample is almost entirely converted into rutile form, whereas for a concentration of Nb equal to 6% the rutile content only reaches a few percent, with an anatase/rutile mixture being observed for intermediate compositions. For concentrations above 6%, we observe a saturation of niobium modifying effect on the anatase-to-rutile transformation; the samples with Nb percentages equal to 8 and 10 at. % contained the same rutile content as the 6% composition for all temperatures. Finally, whatever the niobium content, the TiO_2 phase totally converts to rutile for 800 and 900 °C thermal treatments. As previously stated, for such synthesis temperatures, the $TiNb_2O_7$ phase has been detected by X-ray diffraction for samples with concentrations of 8 and 10%.

To check the solubility of niobium atoms in either anatase or rutile, the unit cell volumes of both phases have been determined as a function of niobium content. We observe that the unit cell volume of anatase for samples synthesized at 600 °C (Figure 6a) continuously increases with niobium content, whereas the unit cell volume of rutile for samples synthesized at 900 °C (Figure 6b) increases from 0% till 6% of niobium and remains constant for higher values of niobium content. This signifies that the solubility of niobium atoms into TiO_2 may be higher for anatase than for rutile phase. According to the volume analyses, XRD, the data from Figure 6 show that Nb is to some extent soluble in TiO_2 up to $x_{\text{nominal}} = 0.1$. X-ray diffraction analyses may also give information on the nature of chemical state of the additive species. Cell parameters were thus calculated by an energy minimization procedure as implemented in the GULP package,[33] where a mean field approach was used to simulate a partial substitution of Ti^{4+} by either Nb^{4+} or Nb^{5+} species. The interatomic potentials used in this study were directly transferred from the literature.[34] The results of the *a* cell parameter calculations (for which such potentials give a better accuracy when compared to *c* parameter) are reported in Figure 7. It should be noted at this point that such results should be taken with caution because the fully ionic model as used here was shown to reproduce only

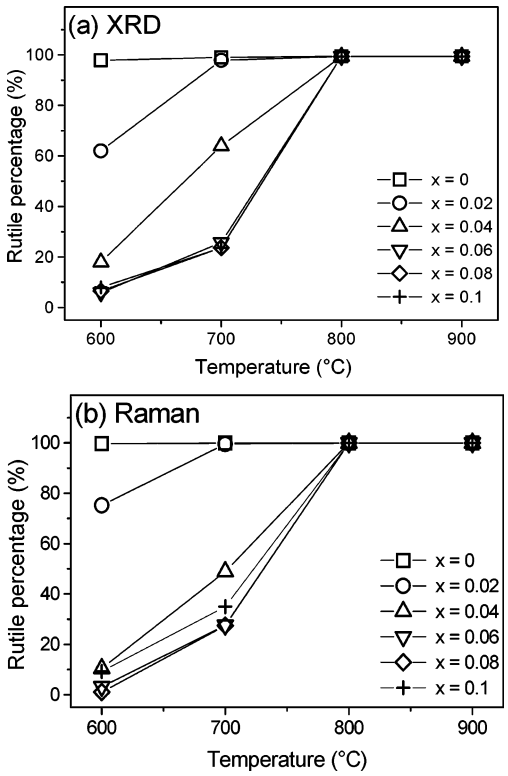

Figure 5. Percentage of rutile (for 100% of TiO_2) as a function of synthesis temperature and Nb/Ti ratio determined from (a) XRD patterns and (b) Raman spectra.

partially TiO_2 anatase and rutile properties. Besides, the mean field approach does not take into account the possible association of defects. Results nevertheless show that the evolution of the *a* cell parameter, in particular in the case of anatase, is better reproduced when Nb is considered to enter both TiO_2 forms in a pentavalent state. Actually, transmission X-ray absorption experiments (not presented here) confirmed that niobium is only present in a pentavalent state. Another supporting evidence that we have indeed Nb atoms spread into anatase is given by the change in the vibration of the Raman modes. As illustrated in Figure 8, the Raman shift of the anatase E_g vibration follows the changes in the lattice parameter, *a*, calculated from XRD for the different concentrations of nominal Nb.

On the other hand, we have also studied the surface chemical composition by means of XPS. In Figure 9, the atomic concentration of Nb over Ti in the surface is plotted against the nominal concentration. The Nb/Ti ratio seen by XPS on the surface increases as the nominal concentration raises. However, there is a saturation of the XPS signal for $x_{\text{nominal}} > 0.08$ for anatase and for $x_{\text{nominal}} > 0.06$ for rutile, suggesting that in these cases the Nb is strongly segregated, i.e., the Nb that is not incorporated into the bulk goes to the surface of the nanoparticles. Both XRD and XPS data agree on this characteristic. In fact, the XPS values are rather higher than the nominal ones, especially for rutile, where an Nb/Ti ratio of 0.4 is measured. Thus, in agreement with the surface analyses, XPS, the data from Figure 9 confirm that there is some concentration of Nb at the surface of the nanoparticles. However, it would be interesting to estimate whether this value is lower or higher than the value inside the nanoparticle, i.e., if there is an accumulation at the surface or there

(33) Gale, J. D. *J. Chem. Soc., Faraday Trans.* **1997**, *93*, 629.
(34) Woodley, S. M.; Battle, P. D.; Gale, J. D.; Catlow C. R. A. *Phys. Chem. Chem. Phys.* **1999**, *1*, 2535.

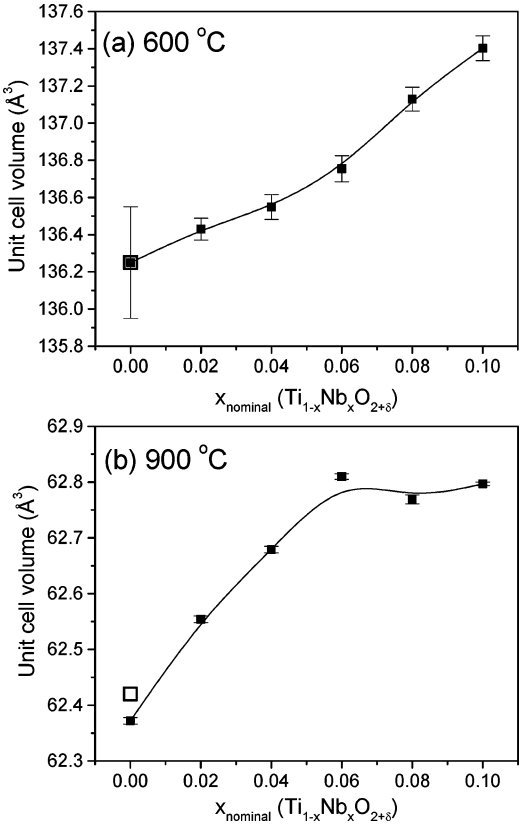

Figure 6. Evolution of unit cell volume as a function Nb/Ti ratio for anatase in the case of sample treated at 600 °C (a), and rutile in the case of samples treated at 900 °C (b) (full squares). Theoretical values of pure anatase (a) and rutile (b) are represented by open squares.

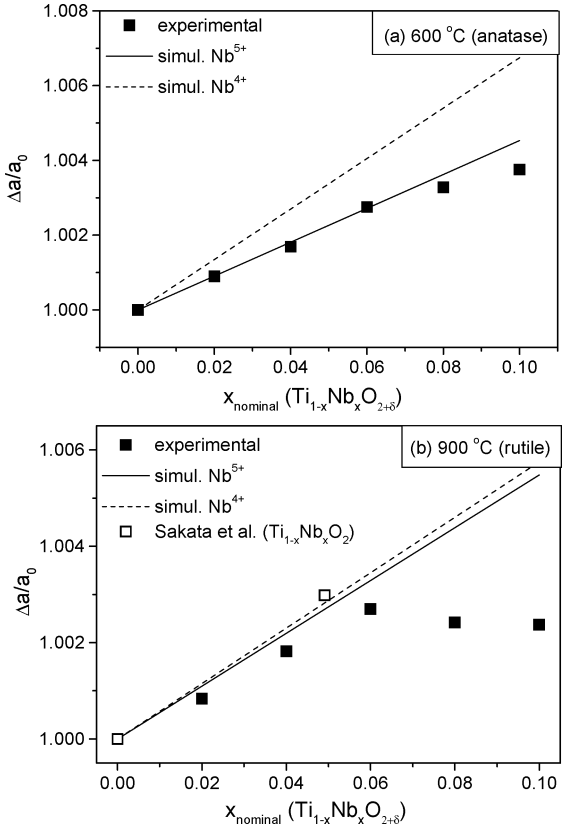

Figure 7. Variation of the *a* lattice parameter as a function Nb/Ti ratio for anatase in the case of sample treated at 600 °C (a), and rutile in the case of samples treated at 900 °C (b) (square symbols). The calculated values depending on the chemical state of the Nb atoms are represented by straight and dotted lines, assuming Nb^{5+} and Nb^{4+} respectively.

is a depletion zone in the value of Nb. These aspects will be discussed in the next section.

To study the band structure and the chemical states of the samples, we analyzed by XPS the core level of the elements and the valence band of the materials. From the core level measurements, we observed that the binding energy (BE) of Ti and O follows the same trend and shifts by the same amount when Nb is introduced. These results are shown in Figure 10, where the BE of the oxygen core level is plotted as a function of the one of titanium for the different Nb contents. From 0−4% of nominal Nb concentration, the BE of Ti and O core levels increases as the Nb content raises, which could be due to a change in the Fermi level position. Figure 11 shows the XPS measurements in the valence band region for the samples calcined at 900 °C. We observed a clear shift to higher binding energies when Nb is present in TiO_2, which supports the fact that there is certainly a change in the Fermi level energetic location.

For titanium, the chemical state observed by XPS has been ascribed to Ti^{4+}. In the case of Nb, the correlation between the peak position and the valence state is not trivial. Figure 12 presents the high-resolution XPS spectra in the Nb3d region for the samples modified with Nb and calcined at 600 and 900 °C. The reference values for Nb^{4+} and Nb^{5+} presented in the figure were taken from ref 24. By comparing with these references, the energetic position and the shape of the peaks at low calcination temperatures, 600 °C, could indicate a mixture of Nb^{4+} and Nb^{5+} states. At high calcination

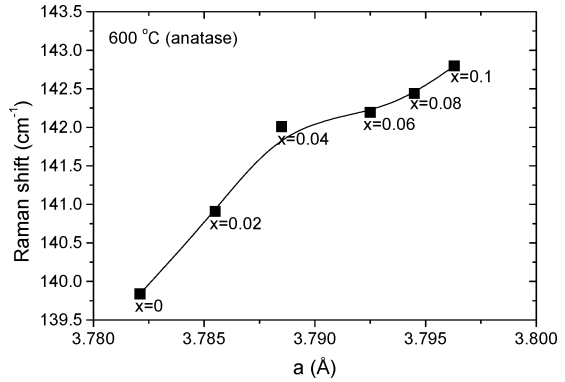

Figure 8. Raman shift of the anatase E_g vibration versus the lattice parameter, *a*, for the samples calcined at 600 °C.

temperatures, 900 °C, the peaks are shifted to higher binding energies, in this case it could be said that pure +5 state is found. Nevertheless, the values extracted from the literature for Nb^{4+} and Nb^{5+} correspond to the Nb 3d binding energy for bulk NbO_2 or Nb_2O_5 samples. In our case, however, the materials are nanocrystalline and, therefore, the Nb 3d BE is determined by the modification of the Fermi level at the surface of the nanoparticle, which is conditioned by the Fermi level at the bulk and the nanograin band bending, which depends on the concentration of surface states. In this regard, Figure 13 highlights how the Nb binding energies follow an evolution similar to that of the Fermi level position for the different Nb concentrations. In this figure is plotted the shift of the band bending energy

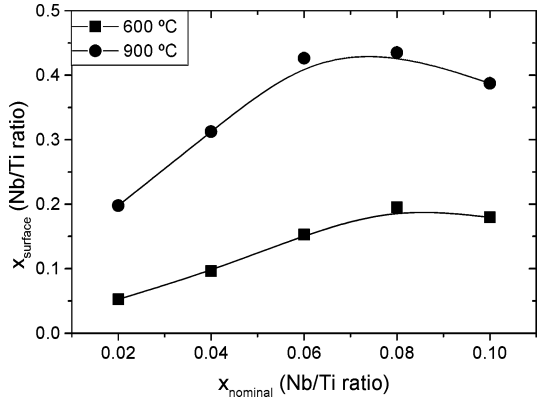

Figure 9. Concentration of Nb on the surface for the samples calcined at 600 and 900 °C in function of the nominal concentration. The surface values have been calculated from XPS measurements.

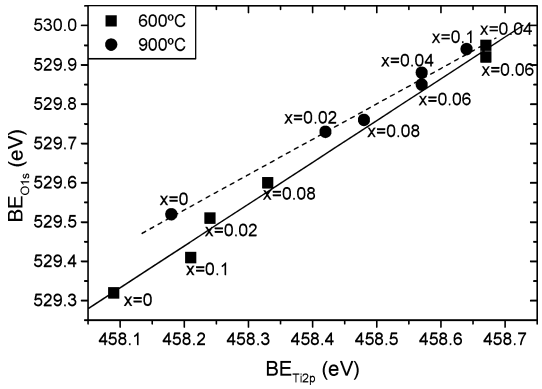

Figure 10. Binding energy of the oxygen related to the titanium for the unmodified and modified samples calcined at 600 and 900 °C.

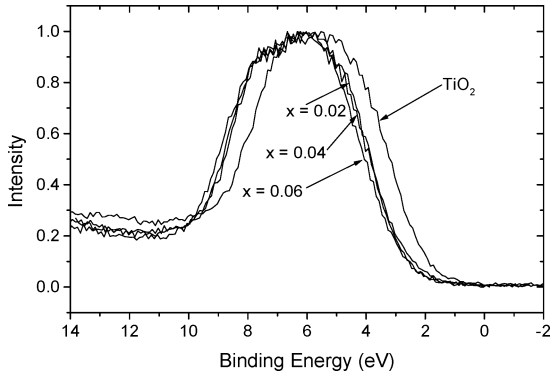

Figure 11. XPS analyses in the valence band region for the bare TiO_2 and the Nb-modified samples with 0.02, 0.04, and 0.06 of Nb contents, *x*, and calcined at 900 °C.

relative to the one for the sample with $x = 0.02$ against the change of the position of the maximum intensity of the Nb binding energy spectra related to the position for $x = 0.02$.

Discussion

The main difficulty of studying Nb-modified TiO_2 samples comes from the lack of thermodynamic data about the $Nb_2O_5-TiO_2$ and NbO_2-TiO_2 pseudo-binary systems, from the existence of various TiO_2 structural forms (brookite, anatase, and rutile) and intermediary compounds, namely $TiNb_2O_7$[35] and $Ti_2Nb_{10}O_{29}$,[36] and finally from the possibility of different oxidation states for either titanium or niobium.

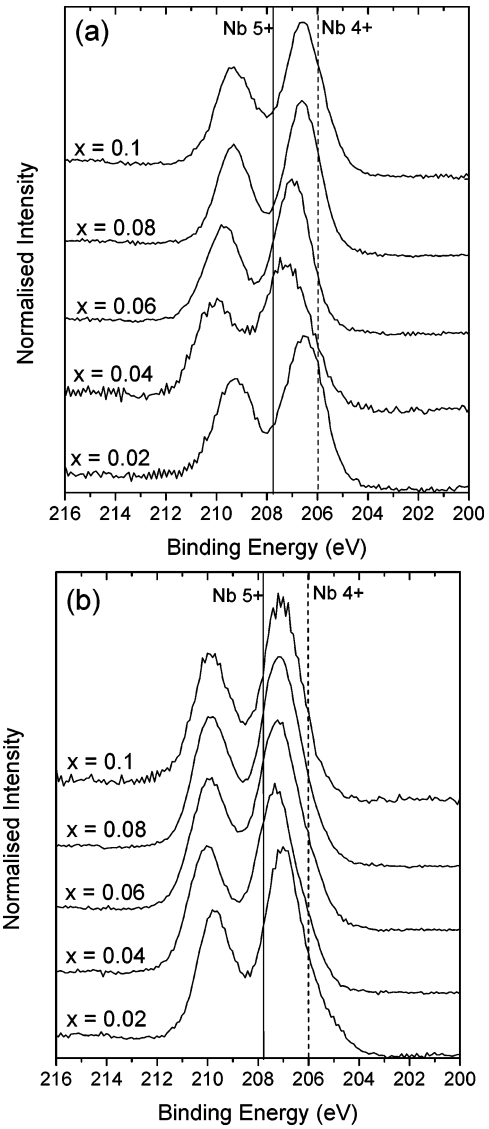

Figure 12. High-resolution XPS spectra in the Nb3d region for the samples with composition $x = 0.02$, $x = 0.04$, $x = 0.06$, $x = 0.08$, and $x = 0.1$, calcined at 600 °C (a) and 900 °C (b). The binding energies of Nb^{5+} (207.8 eV) and Nb^{4+} (206 eV), indicated by solid and dashed vertical lines, respectively, were taken from ref 24 and correspond to a bulk material; though, in our case, the materials are nanocrystalline.

The consequences of the titanium substitution by niobium in TiO_2 in terms of defects, local strain, and electronic properties can be summarized as follows. If we consider that niobium is in its Nb^{4+} oxidation state no mechanism of charge compensation occurs and the following charge equilibrated equation, expressed in the classical Kröger−Vink notation, is produced:

$$NbO_2 + Ti_{Ti}^{x} \rightarrow Nb_{Ti}^{x} + TiO_2 \qquad (3)$$

On the other hand, if we assume that niobium is in its Nb^{5+} oxidation state, the charge compensation of Nb^{5+} in substitution to Ti^{4+} is achieved either by the creation of one Ti cation vacancy per four Nb introduced, or by the stoichiometric reduction of Ti^{4+} to Ti^{3+} per niobium introduced

(35) Wasdley, A. D. *Acta Crystallogr.* **1961**, *14*, 660.
(36) Wasdley, A. D. *Acta Crystallogr.* **1961**, *14*, 664.

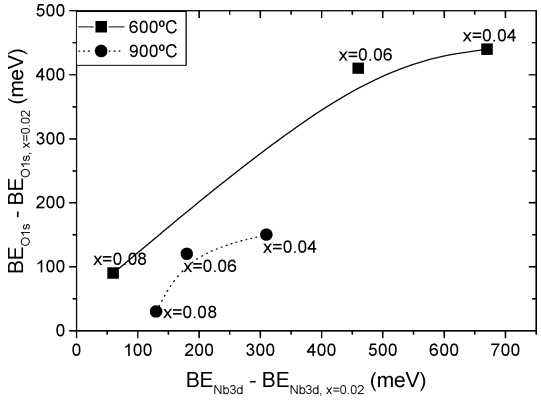

Figure 13. Shift of the band bending energy relative to that shown by the $x = 0.02$ as a function of the change of the Nb XPS peak position versus the value for $x = 0.02$, for the unmodified and some of the modified samples calcined at 600 and 900 °C.

$$\frac{1}{2}Nb_2O_5 + Ti_{Ti}^{x} \rightarrow Nb_{Ti}^{\bullet} + \frac{1}{4}V_{Ti}^{''''} + TiO_2 + \frac{1}{4}O_2 \quad (4)$$

$$\frac{1}{2}Nb_2O_5 + Ti_{Ti}^{x} \rightarrow Nb_{Ti}^{\bullet} + Ti_{Ti}^{'} + \frac{5}{4}O_2 \quad (5)$$

According to the previous works mentioned in the Introduction section, the occurrence of one or other of these scenarios will depend on synthesis conditions, oxygen partial pressure, temperature, niobium concentration, and the energy cost of such defects in the titania structure. Oxidative synthesis conditions and low niobium contents might play in favor of the scenario corresponding to eq 4 because cations would be maintained in their higher oxidation state, whereas scenarios corresponding to eqs 3 and 5 should be considered in reductive synthesis conditions and high niobium concentrations. From qualitative arguments on the steric effect of substitution, the relative radii of titanium and niobium cations in 6-fold coordination, $r(Nb^{4+}) = 0.068$ nm, $r(Nb^{5+}) = 0.064$ nm, and $r(Ti^{3+}) = 0.067$ nm, $r(Ti^{4+}) = 0.0605$ nm,[37,38] seem to play in favor of the pentavalent oxidation state of niobium.

Solubility Limit of Nb into Anatase and Rutile. Total solubility in the TiO_2(rutile)−NbO_2 system has been reported when samples were prepared under reducing condition.[25,27,39,40] Oppositely, for samples prepared in oxidative atmosphere, a demixtion between rutile and $TiNb_2O_7$ phases has been observed for niobium contents higher than $x = 0.06$.[25,26] In this case, niobium is always in its highest oxidation state, and charge compensation occurs via the creation of titanium vacancy. Finally, it has been observed that epitaxy could stabilize a $Ti_{1-x}Nb_xO_2$ rutile phase up to $x = 0.4$ concentration levels, even if treated under oxidative atmosphere.[20−23]

In our case, the powder samples obtained by sol−gel have been treated under oxidative atmospheres and consisted of polycrystalline anatase, or rutile, or a mixture of both phases. The Nb solubility limit found for the rutile structure in our sample, i.e., 6 at. %, is in agreement with the reported data. On the other hand, however, the unit cell volume for anatase expands monotonically as the concentration of Nb is increased, and no segregation of the ternary $TiNb_2O_7$ has been observed in the range of concentrations studied. The amount of Nb that can be accommodated in the anatase was seen to have a saturation point over 10 at. %. This can be related to the differences in topology and elastic properties of anatase and rutile forms as discussed in ref 46.

Inhibition of Crystallite Growth and Anatase-to-Rutile Transfomation. In bare TiO_2, the experimental observation that the anatase-to-rutile phase transformation begins at the surface of the bulk anatase[41] is related to the high tangential diffusion of anatase nanospheres deduced by molecular dynamics simulations.[42] It has been widely accepted that the presence of niobia stabilizes the transformation of anatase to rutile and also the surface area of anatase.[43] The phase transformation hindering can be attributed to the formation of strong Nb−O−Ti bonds, which inhibit the movement of surface Ti atoms required to initiate the phase transformation.[44] The phase transformation rate is also influenced by the amount of oxygen vacancies that act as nucleation sites for the anatase to rutile transition.[45] Arbiol et al.[46] observed that for low Nb contents on titania (up to 4 at. %) niobium was incorporated in TiO_2 thus decreasing the number of oxygen vacancies, which hindered the phase transformation. For higher Nb concentrations, niobium was segregated from the titania lattice, which yielded an increase of the oxygen vacancies and the phase transformation was no longer prevented. Recently, Guidi et al.[47] suggested that the main mechanism for the nucleation of rutile in doped TiO_2 samples was a slow surface nucleation, which also prevented conspicuous grain growth, and ascribed such inhibitions to a decrease in the ionic oxygen mobility.

In titania samples modified with Cr, an effect on crystallite growth hindering and phase transformation inhibition similar to that produced by Nb has been reported.[12] In the case of Cr-doped TiO_2, in which Cr displays a trivalent chemical nature, the oxygen vacancies concentration is not reduced. Consequently, we could assume that the obstruction of the tangential diffusion of anatase nanoparticles is the most important factor that would prevent both mechanisms (crystallite growth and phase transition). Indeed, XPS analyses showed that there is a rather high concentration of Nb on the surface, which could interfere with the diffusion and sintering of anatase nanoparticles during annealing. Furthermore, this is in agreement with the saturation of the niobium content on the surface of the

(37) Shannon, R. D.; Prewitt, C. T. *Acta Crystallogr. B* **1970**, *26*, 1046.
(38) Shannon, R. D. *Acta Crystallogr. A* **1976**, *32*, 751.
(39) Sakata, K. *Acta Crystallogr. B* **1979**, *35*, 2836.
(40) Poumellec, B.; Marucco, J. F. *J. Phys. Chem. Solids* **1985**, *46*, 71.
(41) Shannon, R. D.; Pask, J. A. *J. Am. Ceram. Soc.* **1965**, *48*, 391.
(42) Ogata, S.; Iyetomi, H.; Tsuruta, K.; Shimojo, F.; Nakano, A.; Kalia, R. K.; Vashishta, P. *J. Appl. Phys.* **2000**, *88*, 6011.
(43) Carotta, M. C.; Ferroni, M.; Guidi, V.; Martinelli, G. *Adv. Mater.* **1999**, *11* (11), 943.
(44) Pittman, R. M.; Bell, A. T. *J. Phys. Chem.* **1993**, *97*, 12178.
(45) Hishita, S.; Mutoh, I.; Koumoto, K.; Yanagida, H. *Ceram. Int.* **1983**, *9*, 61.
(46) Arbiol, J.; Cerdà, J.; Dezanneau, G.; Cirera, A.; Peiró, F.; Cornet, A.; Morante, J. R. *J. Appl. Phys.* **2002**, *92*, 853.
(47) Guidi, V.; Carotta, M. C.; Ferroni, M.; Martinelli, G.; Sacerdoti, M. *J. Phys. Chem. B* **2003**, *107*, 120.

materials for $x > 0.06$ (Figure 9). We have stated that the inhibition of crystallite growth and phase transformation was effective until $x = 0.06$. Above this concentration, the crystallites were no more reduced in size and the rutile percentage was quite similar. Likewise, the surface concentration given by XPS exhibits a saturation point at $x = 0.06$ for rutile. Finally, it has been shown that small crystallite size plays thermodynamically in favor of anatase instead of rutile, due to differences in surface energy and surface stress.[48] The smaller crystallite size of Nb-doped samples would then also allow retarding the anatase-to-rutile transformation.

Nb Concentration Profile: Surface and Bulk Composition. As shown by the unit cell volume calculated from XRD (Figure 6) and corroborated by the variation in the vibration modes observed by Raman (Figure 8), there is some Nb inside the TiO_2 lattice. However, not all the Nb is in the bulk of the material, as the lattice parameters found are lower than that expected if all the Nb went substitutional in Ti sites (Figure 7).

XPS measurements showed that there is Nb at the surface (Figure 9) and the concentrations given where rather higher than expected. For instance, at an $x_{nominal}$ of 0.06, the measured value was about 0.15 for anatase (600 °C) and 0.43 for rutile (900 °C). Therefore, it could be stated that the Nb missing from the bulk is located at the surface, yielding a U-shaped Nb concentration profile in the nanoparticle, i.e., there is more Nb at the surface than in the bulk, a fact that is especially significant for rutile, where nearly all the Nb is segregated. The saturation of the $x_{surface}$ at high nominal Nb concentrations (Figure 9) could be due to the strong segregation of Nb and the possible formation of other phases that block the titanium XPS signal. An Nb layer that masks the signal from the Ti below could be covering the TiO_2 nanoparticles from $x_{nominal} > 0.08$ and 0.06 for anatase and rutile, respectively. Consequently, the XPS signal would be very similar above these concentrations.

Band Structure and Chemical Species. It has been observed that the substitutional niobium alters the band structure of titania. On one hand, Nb modifies the band curvature in the TiO_2, as inferred from Figure 10. At 600 °C, the BE of the Ti and the O core levels increases by nearly the same amount upon the incorporation of Nb. The slope of the plot is 1, which indicates that the band bending of titanium due to the Nb addition is the same as that of oxygen. That is, these BE shifts are likely to be Fermi shifts rather than chemical changes; we could state that oxygen is bond to titanium to form TiO_2. Nevertheless, the slope of the plot for the samples calcined at 900 °C is not exactly 1. There is a slightly larger shift for the Ti2p level than for the O1s, suggesting the possibility of a small chemical shift superposed on the main Fermi shift, which is in accordance with the $TiNb_2O_7$ structure observed from XRD. As already stated, though, we should bear in mind that the position of the XPS peaks depends on the Fermi level at the surface, which is influenced by the band bending and the bulk Fermi level. Therefore, these two components contribute to the Fermi shifts inferred from Figure 10.

On the other hand, as shown in Figure 11, the valence band edge of titania is shifted to higher binding energies when Nb is introduced. This displacement of the valence band is due to a donor state introduced in the band gap, which locates the Fermi level closer to the conduction band revealing that the new ternary material formed has a stronger n-type electronic conductivity, likely due to the defects originated by the addition of Nb, such as titanium vacancies or interstitial oxygens. Despite that, we have not observed the new density of occupied states in the band gap of titania that Morris et al. found.[24] Most probably, the electrons introduced by substitutional Nb are located in a band degenerated with the conduction band, as suggested in ref 22.

On balance, it is clear that the Fermi level position is modified as a consequence of the Nb addition. As the concentration of Nb in the bulk increases, the n-type character of the material becomes stronger and the Fermi level approaches the conduction band. Therefore, the energetic distance to the O and Ti levels increases, as observed for low Nb contents in Figure 10, where the BE of Ti and O in effect increases as the Nb/Ti ratio increases until $x = 0.04$. For higher Nb concentration, the segregation of Nb to the surface of the nanoparticle intensifies the density of surface states producing a downward band bending that compensates the position of the O and Ti levels, hence reducing the energetic distance between these levels and the Fermi level position as the band bending increases. This justifies the experimental observation that for high Nb contents the BE of O and Ti levels decreases again, except for rutile at 10% of Nb concentration, where the BE newly increases, probably due to the presence of other phases, such as $TiNb_2O_7$.

Regarding the chemical states, previous XPS and XANES studies[24,27] revealed that, in reducing conditions, for low niobium content ($x < 0.1$), the oxidation state of niobium is mainly Nb^{5+} and charge compensation occurs via Ti^{4+} reduction into Ti^{3+}. For higher concentration levels, niobium is mainly in its Nb^{4+} oxidation state. In oxidizing treatments, the valence states have been reported to be Nb^{5+} and Ti^{4+} and extra charge is compensated by cation vacancies.

As mentioned in the results section, the variation of the lattice parameter in the samples indicated that Nb enters as Nb^{5+} in the bulk (Figure 7). The chemical state observed for Ti was +4. In the XPS spectra we could not distinguish any trivalent titanium. On the basis of these data, we could state that the charge compensation of Nb^{5+} in substitution to Ti^{4+} is achieved by the creation of cation vacancies. However, as the concentration of such Ti^{3+} ions could be small, the main tetravalent state could hinder its detection.

Concerning the valence state of Nb at the surface, it was observed that the Nb 3d peaks shifted to higher BE at 900 °C, as compared to the peaks at 600 °C (Figure 12). Although the spectra in the region $Nb3d_{5/2}$ had to be fitted using the convolution of two peaks, it is risky to ascribe the peak positions in terms of Nb^{4+} and Nb^{5+} components, because different aspects affect the BE position, such as modifications in the band bending, surface states, or Fermi level. Moreover, at high Nb

(48) Zhang, H.; Banfield, J. *J. Mater. Chem.* **1998**, *8*, 2073.

contents, effects due to the segregation of $TiNb_2O_7$ or the possible formation of Nb...Nb pairs that could trap Nb4d[1] electrons and localize them in Nb^{4+} ions (as suggested by Antonio et al.[27]) could also alter the XPS spectra. Anyway, as indicated in Figure 13, it is worth pointing out that the position of the maximum of the Nb peaks is sensitive to the changes of the Fermi level with the Nb content.

Conclusions

The $Nb_xTi_{1-x}O_{2+\delta}$ system has been studied regarding the changes induced by low concentrations of Nb ($x \leq 0.1$) in the structural and electronic properties in order to obtain better knowledge on how Nb modifies the TiO_2 nanomaterial, especially those characteristics that can play a significant role in the gas-sensing mechanisms, such as the crystallite and grain size, bulk conductivity, Fermi level position, surface band bending, surface states, and position and site originated by the presence of Nb atoms. We are currently investigating the consequence of all of these on the sensing characteristics and the discussion will be reported soon.

In agreement with XRD and Raman analysis, some Nb enters in the bulk of the material and is located in substitutional Ti sites assuming a pentavalent nature. The remaining Nb is segregated and/or located at the surface, as suggested by XPS. Such segregation is more conspicuous for rutile than for anatase. In both cases, however, there is more Nb accommodated at the surface than in the bulk. Moreover, a ternary phase ascribed to $TiNb_2O_7$ is segregated when the concentration of Nb exceeds 6 at. % and the annealing treatment is above 800 °C.

In the range of the studied concentrations, the Nb-modified materials have been stabilized from phase transformation and surface area lost. The segregation of Nb to the surface obstructs the diffusion and sintering of anatase particles, therefore impeding crystallite coarsening and phase transition. A saturation of these effects has been observed at 6 at. % content. For Nb contents higher than 6 at. %, the crystallite size and the percentage of phases was very similar at each calcination temperature. Accordingly, this is the same concentration at which the amount of Nb in the surface of rutile also reaches saturation, as inferred from XPS measurements.

Concerning electronic states characterization, Nb^{5+} was always present in all the samples and trivalent titanium has not been found in any case, which suggests that charge compensation is done via cation vacancies. Considering any new band gap state has been detected due to the incorporation of Nb, it is reasonable to assume that the extra valence Nb electrons donated to the system are located in a band degenerated with the valence band, as suggested by previous works.[22]

The Nb-modified materials exhibited stronger n-type character and higher electronic conductivity. The introduction of niobium into titania may lead to an increase in the concentration of electrons as well as induce the creation of a donor level by the formation of defects, such as titanium vacancies or interstitial oxygens, which shifts the Fermi level toward a location closer to the conduction band, as observed from XPS core level and valence band measurements. This scenario is believed to modify the sensing mechanisms; particularly a different catalytic role is expected for the site defined by the presence of Nb atoms in different places.

Acknowledgment. E.M.E. is a member of CEMIC (Centre of Microsystems Engineering) and CeRMAE (Reference Centre of Advanced Materials for the Energy). We thank the Spanish CICYT program MAT 99-0435-C02-01 and the Spanish FEDER program 2FD1997-1804-C03-01 for financial support.

CM0351238